Enhancement of energy release performance of Al–Ni composites by adding CuO

Caimin Huang, Jin Chen, Shuxin Bai, Shun Li, Yu Tang, Xiyue Liu, Yicong Ye, Li'an Zhu

PII: S0925-8388(20)31634-0

DOI: https://doi.org/10.1016/j.jallcom.2020.155271

Reference: JALCOM 155271

To appear in: *Journal of Alloys and Compounds*

Received Date: 25 January 2020

Revised Date: 16 April 2020

Accepted Date: 18 April 2020

Please cite this article as: C. Huang, J. Chen, S. Bai, S. Li, Y. Tang, X. Liu, Y. Ye, Li'. Zhu, Enhancement of energy release performance of Al–Ni composites by adding CuO, *Journal of Alloys and Compounds* (2020), doi: https://doi.org/10.1016/j.jallcom.2020.155271.

CRediT author statement

Caimin Huang: Conceptualization, Formal analysis, Writing-Original Draft.

Jin Chen: Methodology, Data curation, Visualization.

Shuxin Bai: Funding acquisition, Methodology, Investigation, Supervision.

Shun Li: Funding acquisition, Formal analysis, Resources, Writing-review& editing.

Yu Tang: Data curation, Formal analysis, Writing- original draft, Writing-review & editing.

Xiyue Liu: Formal analysis, Data curation.

Yicong Ye: Project administration, Formal analysis, Validation.

Li'an Zhu: Formal analysis, Validation.

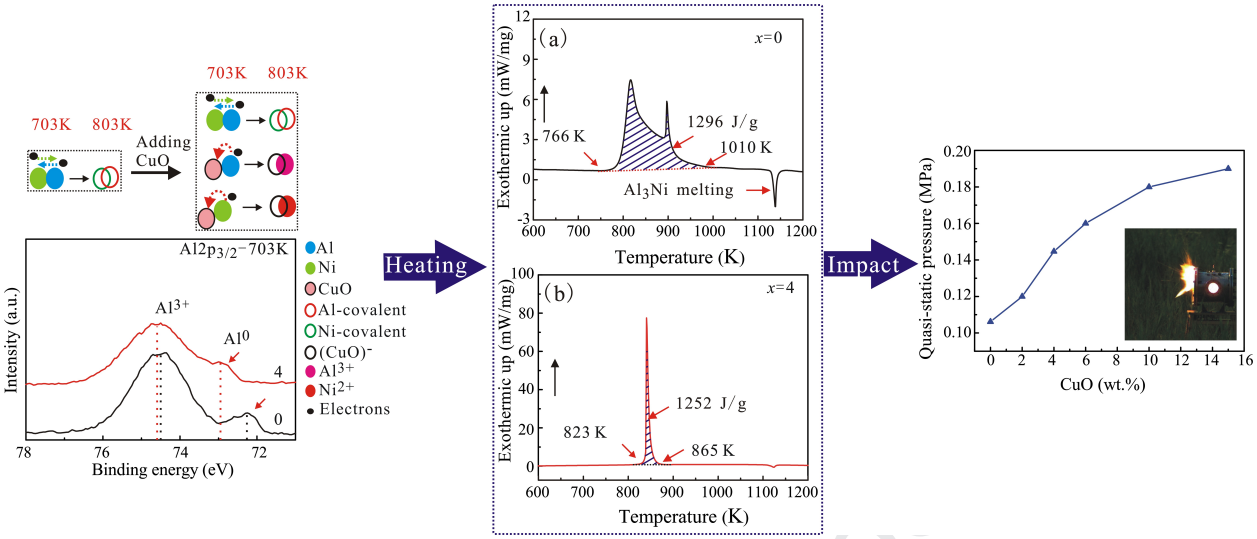

Enhancement of energy release performance of Al–Ni composites by adding CuO

Caimin Huang [a], Jin Chen [b], Shuxin Bai [a], Shun Li [a,] *, Yu Tang [a,] *, Xiyue Liu [a], Yicong Ye [a], Li'an Zhu [a]

[a] *Department of Materials Science and Engineering, College of Aerospace Science and Engineering, National University of Defense Technology, Changsha 410073, China*

[b] *Xi'an Modern Chemistry Research Institute, Xi'an 710065, China*

*Corresponding authors.

E-mail addresses: linudt@163.com (Shun Li); tangyu15@zju.edu.cn (Yu Tang).

Abstract

Al–Ni composites, which have excellent energy densities and mechanical properties, are promising novel energetic materials for improving the damaging effects of ammunition. To enhance their energy release performance under impact loading, CuO was introduced to form the thermite. The results of differential scanning calorimetry (DSC), heat treatment, and ballistic tests indicated that Al and Ni were more prone to donate their free electrons after the addition of CuO. A decrease in the number of free electrons as well as the weak metal-oxygen bonds at the Al/Ni interfaces caused by the thermal decomposition of CuO, impeded the activity of the Al–Ni intermetallic formation reaction, increasing its onset temperature from 766 K to 820 K. The reduced difference in the onset temperatures for the intermetallic formation and thermite reactions caused the thermite reaction between Al and CuO to be ignited by the Al–Ni intermetallic formation reaction. The overlap of these two exothermic reactions greatly improved the reaction intensity, and then accelerated the oxidation of Al and Ni, finally enhancing the energy release performance during high-speed impact. This work demonstrated that the energy release performance of Al–Ni composites can be effectively modulated by introducing a metal oxide. Moreover, the effect of a metal oxide on the energy release behavior of Al–Ni composites accounted for the interaction of aluminum and nickel with the added copper oxide.

Keywords: Energetic structural materials; Thermite; Al–Ni composites; Energy release performance

1. Introduction

Energetic structural materials (ESMs) are a novel class of energetic materials because of the integration of structural and energetic characteristics. Their distinctive properties support potential use in military applications, such as reactive shaped charges, reactive fragments, reactive armors, and reactive bullets [1-4]. ESMs are generally designed to release energy and are distinguished from traditional energetic materials only by their increased strength [5]. ESMs are incapable of ignition or detonation under ambient conditions [6, 7] and can be initiated during violent impact [8]. The significant heat generated from chemical reactions, e.g., oxidation, the formation of intermetallics and thermite reactions, usually causes significant secondary damage. The amount and rate of released energy play important roles in enhancing the damaging effects of ammunition.

At present, typical ESMs, such as metal thermites, metal-polymer composites, intermetallic-forming composites, and combustible metals, have been studied extensively. Among them, Al–Ni composites have attracted attention due to their high strength (266 MPa [9]), which is much higher than that of Al/PTFE (polytetrafluoroethylene) (35 MPa [10]) and Al/Cr_2O_3 (7 MPa [11]). However, the heat of the intermetallic formation reaction in Al–Ni composites is relatively low (1.38 kJ/g [12]) in argon, and is lower than that of TNT (detonation heat: 4.1 kJ/g [13] and enthalpy of combustion: 14 kJ/g [14]). In addition, Al–Ni composites often partially react under shock and impact loading [9, 15-17], leading to a further decrease in their energy release performance and damaging effects. Therefore, it is important and significant to improve the energy release performance of Al–Ni composites. It is notable that the heat of combustion of Al can be as high as 31 kJ/g [18]; thus, improving the degree and rate of the intermetallic formation reaction and/or combustion reaction of Al–Ni composites enhances their energy release ability.

To reach this goal, efforts have been made, such as the addition of PTFE which

promoted the energy release ability of the composite by participating in the reaction, but it severely impaired the mechanical properties [9]. Moreover, introducing pure metals, including Cu, Mo, and Mg [9, 19], reduced the energy-releasing ability since they cannot participate in the reaction and prevented direct contact between the Al and Ni particles. Therefore, it is necessary to develop an effective method to improve the energy release performance of Al–Ni composites.

It is well known that metal thermites, especially the mixtures of Al and metal oxides, have been broadly applied in propulsion and thermal batteries due to a high theoretical heat of reaction [20]. The theoretical energy densities of the thermite reaction for Al–CuO, Al–Bi_2O_3, and Al–MoO_3 are 4.07, 2.12, and 4.70 kJ/g, respectively [18]. In addition, the burning rates of unconfined Al–CuO, Al–Bi_2O_3, and Al–MoO_3 nanocomposite mixtures (stoichiometric ratios) are 340, 420 and 1000 m/s, respectively [21], as measured by a high-speed camera under ambient pressure and temperature conditions. Furthermore, the heat released in experiments involving the Al-Ni system was affected by oxide additives. For instance, Hashemabad et al. reported that the heat of reaction in an Al-Ni composite increased as the CuO or Fe_2O_3 content increased [22]. However, there is a lack of understanding of the mechanisms responsible for this behavior. Importantly, Dean et al. [23] revealed that the reactions in Al–Ni composites were hindered and even ceased when the MoO_3 content increased to 10 wt.%. That is, the effect of metal oxides on the reactions in Al–Ni composites is uncertain and requires additional research.

In this work, Al-Ni composites (Al: Ni = 48 wt.%: 52 wt.%) were used. CuO with mass fractions of x= 0, 4, 6, 10, and 15 wt.% were added, hereinafter referred to as $(48Al–52Ni)_{100-x}(CuO)_x$. The microstructures, mechanical properties and energy release of the $(48Al–52Ni)_{100-x}(CuO)_x$ composites were investigated in detail. The effects of the metal oxide on the reaction behaviors of the Al–Ni composites and their related mechanisms are revealed. An effective method to modulate the performance of Al–Ni composites as ESMs was determined and demonstrated.

2. Experimental procedures

The $(48Al–52Ni)_{100-x}(CuO)_x$ composites were fabricated first by high-energy ball milling Al (spherical, 5 μm, purity: 99.9%), Ni carbonyl (spherical, 5 μm, purity: 99.8%), and CuO (flake-like, 2–10 μm, purity: 99.5%) powders. The ball-to-powder mass ratio was approximately 10:1. The raw powders were mixed for 20 min at 250 r/min in argon to avoid mechanical alloying. To distinguish this process from mechanical alloying that is mostly generated by high-energy ball milling, this blending process is referred to as mechanical mixing in this work. A small amount of ethyl alcohol was added into the mixtures to prevent cold welding. Importantly, Al, Ni and CuO particles were mixed simultaneously to form composites with CuO. The morphologies of the raw and mixed powders are shown in Fig. S1. Subsequently, the mixtures were dried for 2 h at 343 K in a vacuum oven and then pressed into a steel mold with an inner cavity size of 50 mm × 30 mm × 13 mm under a pressure of 600 MPa at 673 K for 2 h. The hot-pressed composites were machined into cylindrical samples (Φ10 mm × 10 mm) for subsequent experiments. Some samples were annealed at 770, 780, and 790 K for 10 min in sealed quartz tubes in high-purity argon, followed by quenching in water. In addition, dish-like samples with a thickness of 0.3 mm prepared by hot-pressing were used for thermal analysis tests.

The microstructure of the composites was determined by X-ray diffraction (XRD, Smartlab 9KW) with Cu Kα radiation (λ = 1.5406 Å) and scanning electron microscopy (SEM, JSM-6490LV) augmented with energy-disperse spectroscopy (EDS). X-ray photoelectron spectroscopy (XPS) was performed using an EscaLab Xi+ with Al Kα rays (1486.6 eV). A binding energy of 284.8 eV for the C1s peak was used for calibration. Thermal analysis was accomplished through thermogravimetric and differential scanning calorimetry (TG–DSC) (STA449F3, Jupiter, NETZSCH). The samples (approximately 6–10 mg) were heated to 1273 K at a heating rate of 10 K/min in a high-purity argon atmosphere (40 mL/min).

Quasi-static compressive tests were performed using an Instron 3369 testing system at a strain rate of $10^{-3}\cdot s^{-1}$. Ames [24] reported that the amount of released energy can be calculated from the pressure change inside a sealed container. The energy release behaviors were measured by ballistic tests in this work (Fig. 1). The

samples were fixed in nylon sabot and then embedded into steel case (Fig. 1(a)), i.e., projectiles were fabricated. The projectiles were fired by a 14.5 mm caliber gun placed approximately 15 m from the impact target. The pressure changes were recorded by a pressure sensor (PCB 113B26) with a voltage sensitivity of 1413 mV/MPa. The energy release phenomena were also captured with a high-speed camera with a framerate of 2000 fps.

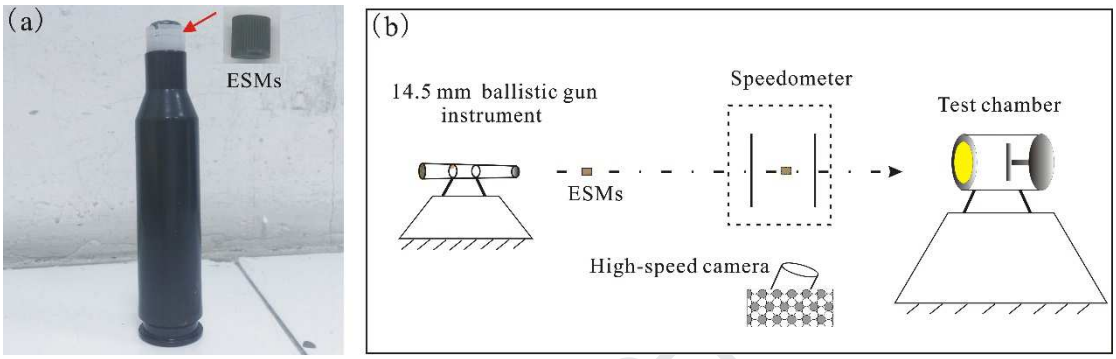

Figure 1. Schematic diagram of ballistic tests (a) projectile; (b) ballistic tests.

3. Results

Fig. 2 presents the XRD patterns and backscattered electron (BSE) images of the hot-pressed $(48Al–52Ni)_{100-x}(CuO)_x$ composites. Obviously, diffraction peaks corresponding to Al, Ni, and CuO were observed in Fig. 2(a). The BSE images (Fig. 2(b–e)) and elemental mapping images (Fig. S2) show that the Al particles underwent significant plastic deformation and formed a continuous matrix, while the Ni and CuO particles tended to connect with each other. It should be noted that the microstructure of the composites with different CuO contents was very similar shown in Fig. 2(b–e).

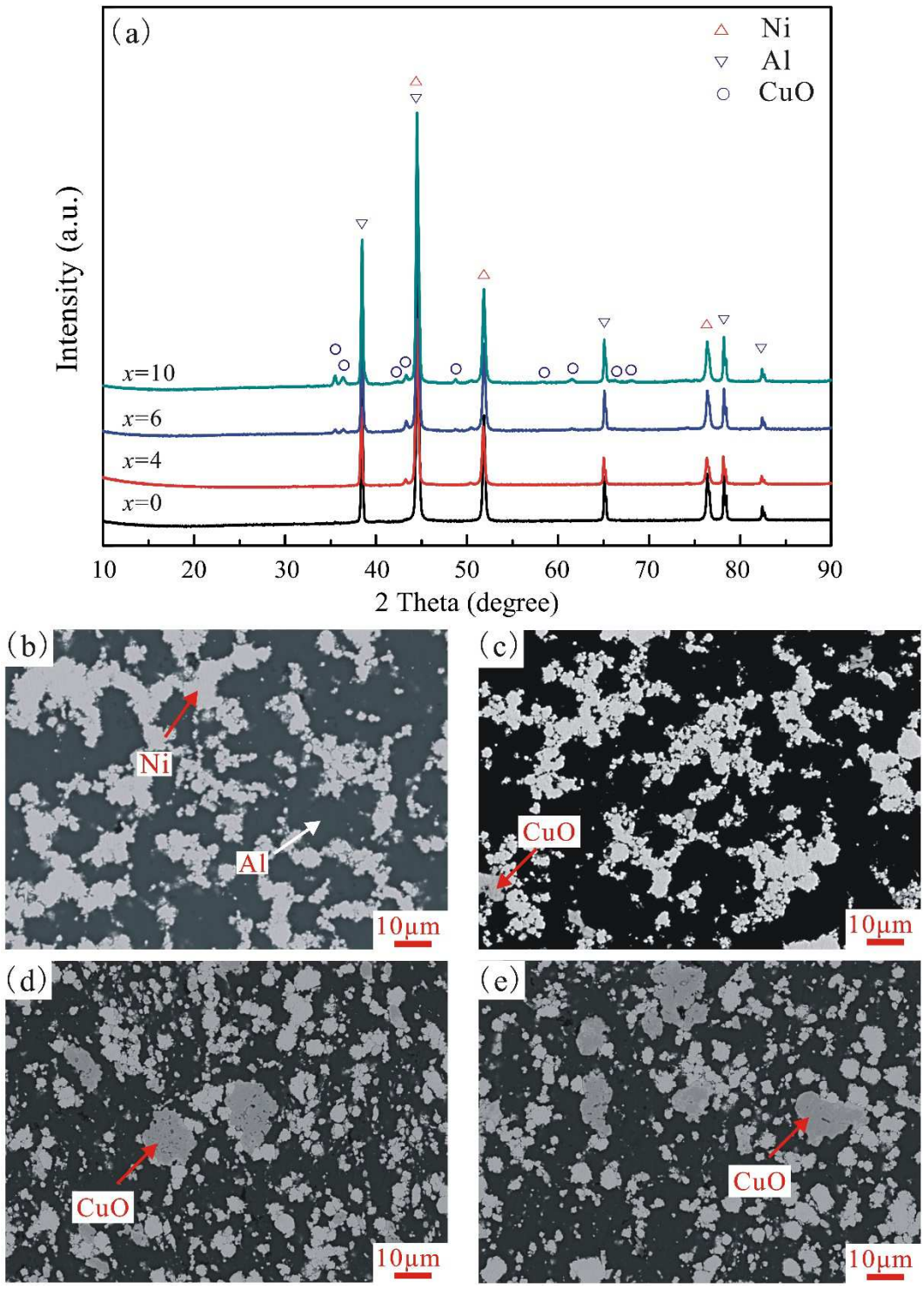

Figure 2. (a) XRD patterns and BSE images of the hot-pressed (48Al–52Ni)$_{100-x}$(CuO)$_x$ composites. ((b) x = 0; (c) x = 4; (d) x = 6; (e) x = 10.

Fig. 3 shows the XPS data of the Al2p$_{3/2}$, Ni2p$_{3/2}$, O1s, and Cu2p spectra from the (48Al–52Ni)$_{100-x}$(CuO)$_x$ composites after annealing at 703 and 803 K. At 703 K, two peaks at 72.8 eV and 74.6 eV, which were assigned to Al^0 (metal Al) [25, 26] and Al^{3+} (Al_2O_3) [27, 28], respectively, can be seen in Fig. 3(a). When CuO was added,

the relative intensity of the Al^0 peak decreased, and the peak position shifted towards a higher binding energy. Similar trends were observed in the $Ni2p_{3/2}$ spectrum. The CuO additive also decreased the relative intensity of the Ni^0 peaks (852.6 eV) [29] and shifted the peak position of Ni^{2+} (854.1 eV) [30]. However, the relative intensity and position of the $Al2p_{3/2}$ and $Ni2p_{3/2}$ peaks did not obviously change as the CuO content increased, as shown in Fig. 3(a) and (c). Moreover, the O1s peaks also slightly shifted towards higher binding energies when CuO was added. However, the Al^0 and Ni^0 peaks from the $(48Al–52Ni)_{100-x}(CuO)_x$ composites disappeared after annealing at 803 K. The Al^{3+} and Ni^{2+} peaks from the composites (x = 4, 10, and 15) shifted to higher binding energies compared with those from the composite (x = 0). In addition, Cu^{2+} peaks disappeared and were replaced by Cu^+ peaks. There was a difference in the charge distribution state of the composites annealed at 703 and 803 K.

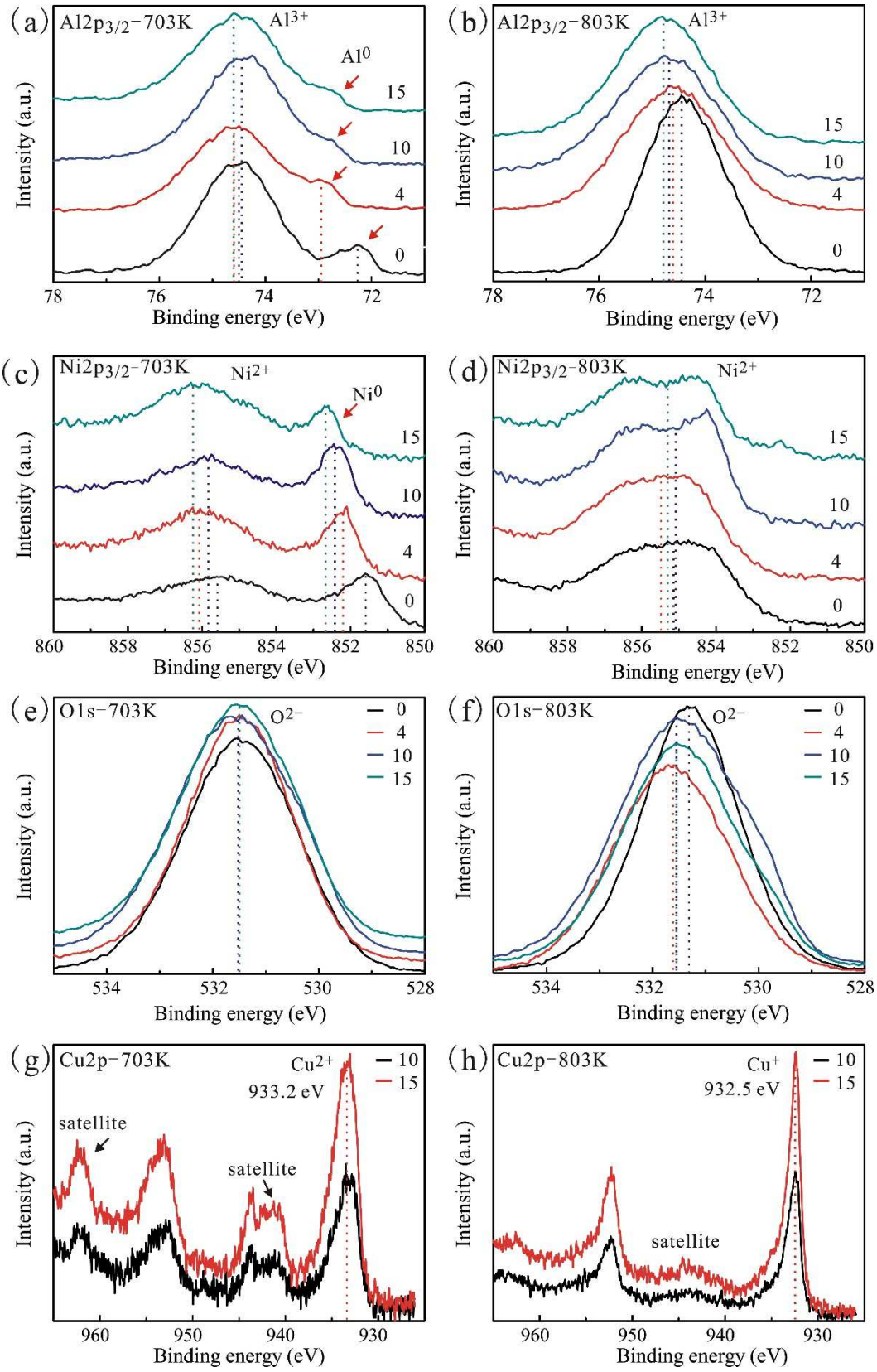

Figure 3. XPS patterns of $Al2p_{3/2}$, $Ni2p_{3/2}$, O1s, and Cu2p spectra of $(48Al–52Ni)_{100-x}(CuO)_x$ composites after annealing at 703 and 803 K, respectively. (a–b) $Al2p_{3/2}$; (c–d) $Ni2p_{3/2}$; (e–f) O1s; (g–h) Cu2p.

Fig. 4 shows the DSC and TG curves of the $(48Al–52Ni)_{100-x}(CuO)_x$ composites in argon. The composite (x = 0) exhibited two overlapping exothermic peaks and one endothermic peak between 600 and 1200 K (Fig. 4(a)). The onset temperature of the exothermic reaction was 766 K. As CuO was added into the composites, only a sharp exothermic peak was observed (Fig. 4(b–c)). The reaction onset temperatures increased to approximately 820 K as the CuO content increased to 4 and 6 wt.%. That is, the exothermic reactions in the composite were delayed by the addition of CuO. Moreover, the heat flow was greatly enhanced after the introduction of CuO, as indicated by the shift in the energy release peaks of the composites from 7.5 mW/mg to 80 mW/mg. In particular, compared to the behavior of the composite (x = 0), a shortened reaction temperature interval and higher heat flow for the composite (x = 4) did not impair the heat of reaction, although the reaction onset temperature increased. The sharply increasing heat flow is likely indicative of the temperature runaway and thus of the reaction proceeding without temperature control. This phenomenon implies that the reaction mechanism of the composites with CuO is different from that of the composite without CuO.

In addition, TG traces of the composites (x = 0 and 6) are shown in Fig. 4(d). Compared to the mass of the composite (x = 0), the mass of the composite (x = 6) decreased significantly at 550–870 K, suggesting that the composite (x = 6) was prone to thermal decomposition and/or the formation of volatile matter.

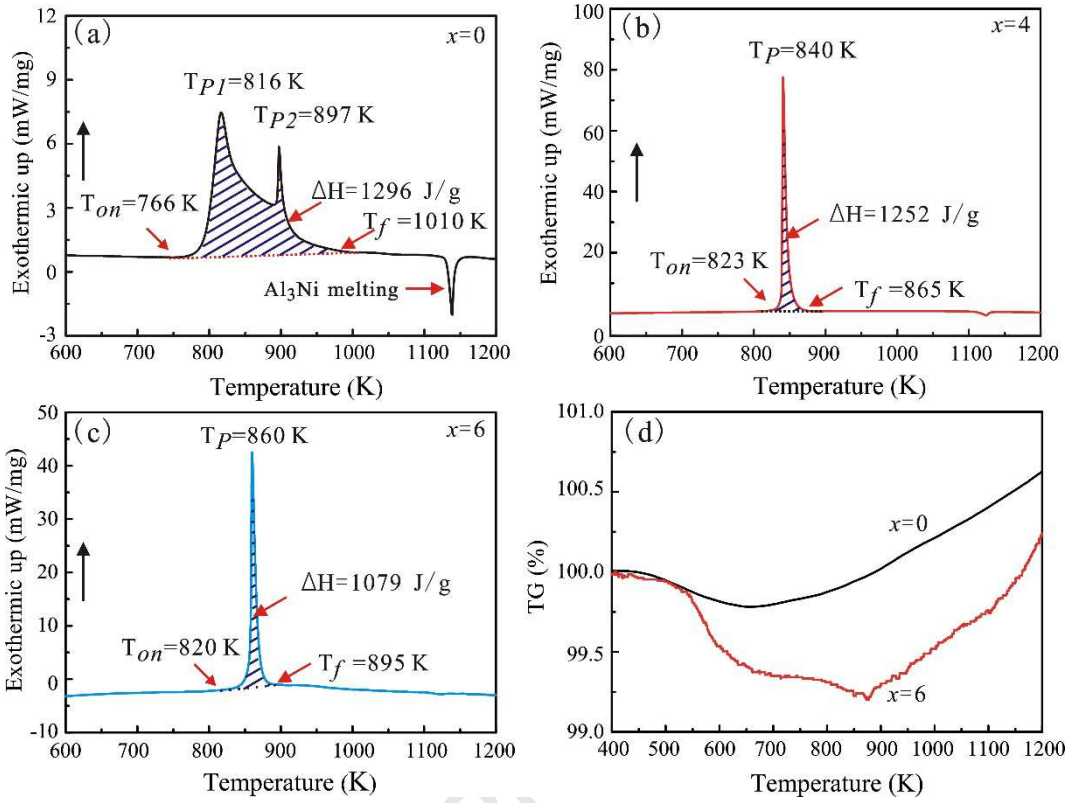

Figure 4. DSC curves of $(48Al–52Ni)_{100-x}(CuO)_x$ composites ((a) x = 0; (b) x = 4; (c) x = 6) and (d) TG curves of the composites (x = 0, 6).

To further investigate the effect of CuO on the exothermic reaction behaviors in Al–Ni systems, the $(48Al–52Ni)_{100-x}(CuO)_x$ composites were quenched at 770, 780, and 790 K, which are higher than the reaction onset temperature of the composite (x=0) (Fig. 4(a)). Fig. 5(a–e) presents the microstructures of the quenched $(48Al–52Ni)_{100-x}(CuO)_x$ composites. As shown in Fig. 5(a), the composite (x=0) completely reacted at 770 K, and the reaction products were identified as Al_3Ni and Al_3Ni_2. However, a large amounts of Al, Ni, and CuO were detected in the XRD patterns of the composite (x=6) after annealing at 770 K. Similar results were observed in the BSE images. All constituents of the $(48Al–52Ni)_{100-x}(CuO)_x$ composites (x=6) remained separate when annealed at 770 K (Fig. 5(b)), while the reaction between Al and Ni occurred at an annealing temperature of 780 K (Fig. 5(c)). Certain intermetallic compounds formed, including Al_3Ni_2 (region B) and Al_3Ni (region C), whereas Al (region D) and Ni (region A) metal particles remained. Moreover, CuO particles also participated in the reaction, and a certain amount of Cu_2O formed at the

boundary of CuO particles, as shown in Fig. 5(d). When the annealing temperature reached 790 K, the Al and Ni in the composite (x=6) completely reacted to form intermetallics, and some Cu dissolved into the crystalline intermetallic compounds, as shown in Fig. 5(e). However, CuO, Cu_2O, and Al were found in the Al–CuO composite after annealing at 790 K (Fig. S3).

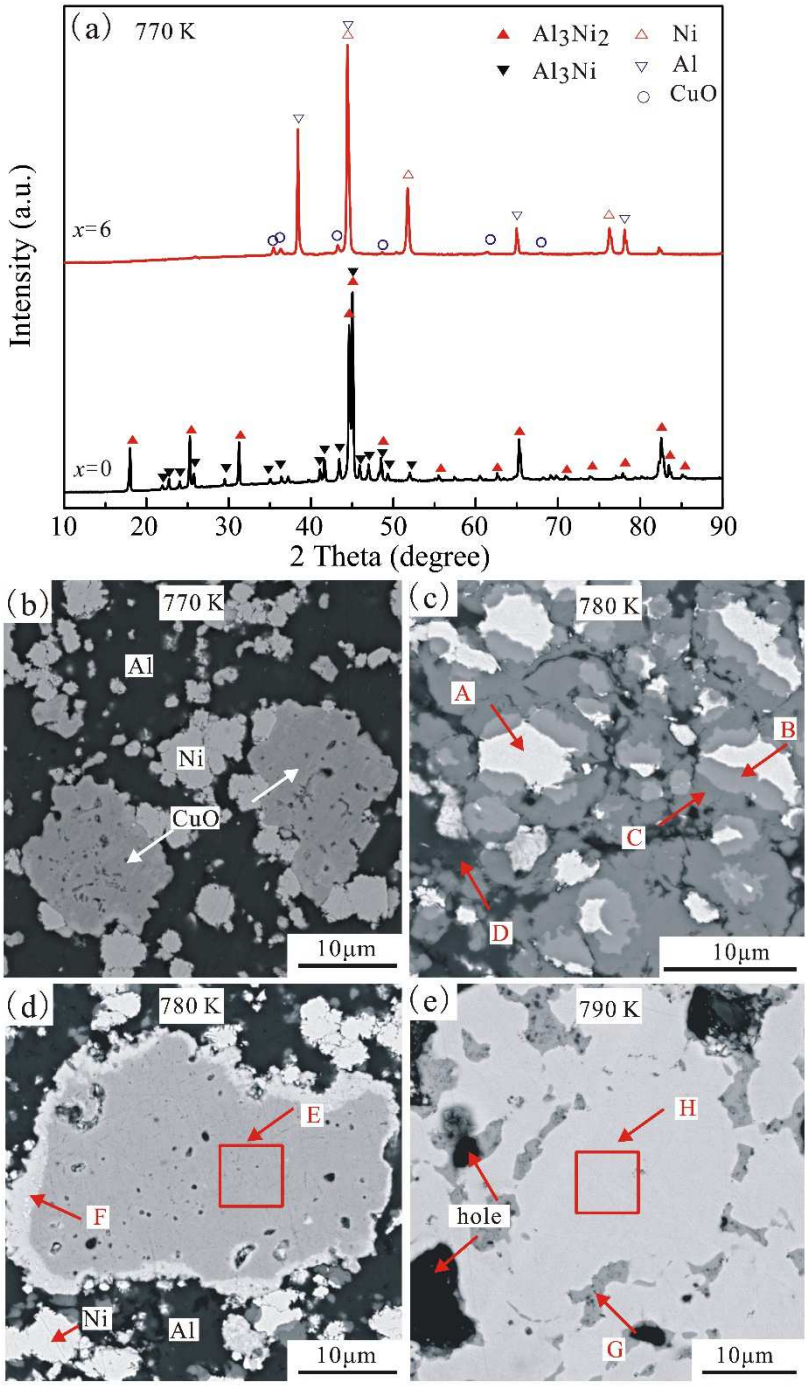

Element	A	B	C	D	E	F	G	H
Al (at.%)	3.17	65.10	78.04	95.15	1.10	1.34	73.35	57.59
Ni (at.%)	96.83	33.49	21.25	1.34	1.16	2.12	25.29	37.77
Cu (at.%)	–	1.41	0.71	–	47.23	62.14	1.36	4.34
O (at.%)	–	–	–	–	50.51	34.40	–	–

Figure 5. Microstructural features of $(48Al–52Ni)_{100-x}(CuO)_x$ composites. (a) XRD patterns of the composites (x= 0, 6) annealed at 770 K; (b) BSE image of the composite (x= 6) annealed at 780 K; (c–d) BSE image of the composite (x = 6) annealed at 780 K; (e) BSE image of the composite (x= 6) annealed at 790 K.

Fig. 6 presents the energy release behavior of the composites during the ballistic tests. As shown in Fig. 6(a–d), once the composites impacted a steel target and penetrated into the tested chamber, a bright emission was captured, indicating that a large amount of heat was generated from impact loading. Moreover, an increase in the quasi-static pressure inside the sealed tested chamber occurred, indicating an increased temperature caused by an energy release. As shown in Fig. 6(e–g), all quasi-static pressure curves of the composites with different CuO contents sharply increased to a maximum within ten milliseconds, and then gradually decreased to ambient pressure due to a venting effect caused by the projectile penetration of the target [31]. However, the peak pressures and pressure increase rates of these composites were different. As the CuO content increased from 0 to 15 wt.%, the peak pressure increased from 0.106 to 0.191 MPa, respectively. The pressure increase rate calculated from the early linear stage (approximately 5–10 ms) of the quasi-static pressure curves, increased from 0.014 to 0.029 MPa/ms at 1400 m/s, as shown in Fig. 6(h).

Fig. 7 presents the XRD patterns and BSE images of the recovered fragments collected from inside the test chamber after impact at 1400 m/s. In general, the recovered fragments included unreacted (Fig. S5), partially reacted, and fully reacted particles. As shown in the XRD patterns (Fig. 7(a)), Al_3Ni and Al_3Ni_2 were detected, and some Al and Ni remained. Moreover, weak diffraction peaks identified as Al_2O_3 and a broad hump at approximately $2\theta = 20°$ were identified as nylon. Similar phenomena were observed in the BSE images. As shown in Fig. 7(b), Al_3Ni, Al_3Ni_2, and Ni were found in the composite (x=0). In contrast, in the composite (x=4) (Fig. 7(c)), only Al_3Ni and Al_3Ni_2 intermetallics were found, and the Ni metal disappeared.

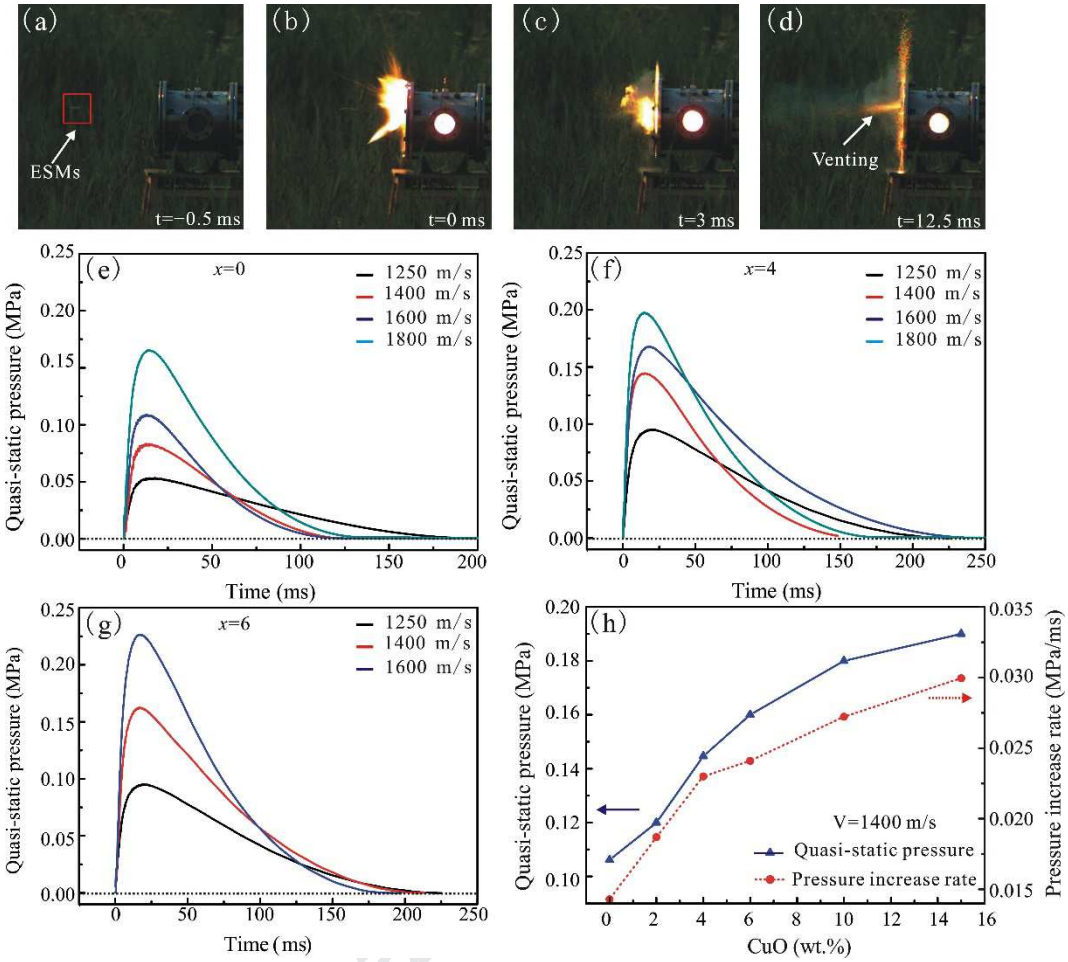

Figure 6. Energy release behaviors under high-speed impact loading. (a–d) Light emission captured by a high-speed camera for the composite (x = 4) at 1400 m/s; (e–g) Quasi-static pressure inside test chamber for the composites with x= 0, 4 and 6, respectively; (h) Relationship between peak pressure, pressure increase rate and the CuO content at 1400 m/s.

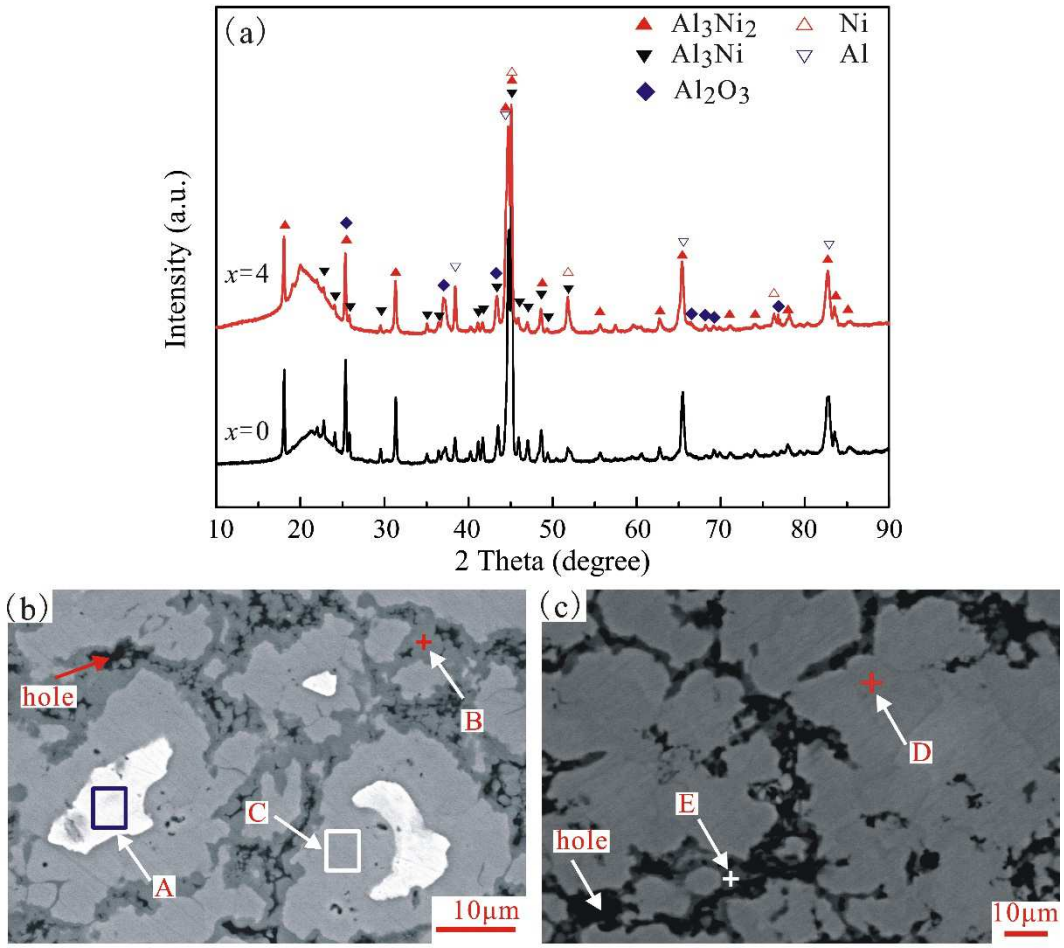

Element	A	B	C	D	E
Al (at.%)	3.96	74.92	63.84	64.89	73.86
Ni (at.%)	96.04	25.08	36.16	33.21	23.68
Cu (at.%)	–	–	–	1.90	1.45
Phase	Ni	Al_3Ni	Al_3Ni_2	Al_3Ni_2	Al_3Ni

Figure 7. (a) XRD patterns of recovered fragment at 1400 m/s; (b–c) BSE images of reacted recovered fragments for the composites with x = 0 and 4, respectively.

4. Discussion

According to previous reports, Al can react with Ni at high temperatures and finally form certain intermetallic compounds [32]. The reaction onset temperature of the Al–Ni system is approximately 913 K [33, 34]. In addition, the ignition temperature of Al–CuO thermite is dependent on the particle size, interface and external conditions. For micron-sized Al–CuO thermite, the reaction onset temperatures of the thermite with a layered structure (Al: ~1 μm, CuO: <5 μm) and

mixture of powders (Al: 44 μm, CuO: 5 μm) were beyond 770 K, as measured by DSC at a heating rate of 5–15 K/min under an argon atmosphere [35, 36]. These reaction onset temperatures are higher than the hot-pressing temperature (673 K). Therefore, the reactions between the Al–Ni system and Al–CuO thermite in the hot-pressed composites were suppressed. The prepared composites only consisted of Al, Ni, and CuO, as shown in the XRD patterns and BSE images (Fig.2). The microstructure of the composites hardly changed when the CuO content increased from 0 to 10 wt.% due to the absence of a chemical reaction. Thus, the similar microstructures of the $(48Al–52Ni)_{100-x}(CuO)_x$ composites caused similar mechanical properties, even though they had different CuO contents (Fig. S3).

Although the addition of CuO did not obviously affect the microstructures or mechanical properties of the $(48Al–52Ni)_{100-x}(CuO)_x$ composites, it did alter the charge distribution of the pure metal. As is known, both Al and Ni have strong reducibility, i.e. they readily lose electrons. When CuO was added into the Al–Ni composites, some electrons left the Al and Ni lattices and moved into the CuO lattice, as demonstrated by the shift in the $Al2p_{3/2}$ and $Ni2p_{3/2}$ peak positions to higher binding energies in Fig. 3. Then some O^{2-} was excluded from the CuO lattice sites to maintain electric neutrality and were reduced to O atoms, manifesting as a blueshift (i.e., the O1s peaks shifted to a higher binding energy after the introduction of CuO).It should be noted that the charge transfer process without an external electrical field is a short-range migration and mainly occurred at the Al/CuO and Ni/CuO interfaces, i.e., the number of transferred charges directly depended on the contact area of the Al/CuO and Ni/CuO interfaces. A larger interfacial area allowed additional charge transfer. As the CuO content increases, the Al/CuO and Ni/CuO interfacial contact area inevitably increases if the CuO particles are distributed homogeneously in the composite. However, CuO aggregated in the composites herein, as shown in Fig. 2(b–e), resulting in only a slightly increased interfacial contact area. This means that increasing the CuO content did not significantly increase the charge transfer in the composites and then did cause a stable peak position in the XPS spectrum for the (48Al–

52Ni)$_{100-x}$(CuO)$_x$ composites with x = 4–15.

Chemical reactions are essentially charge transfer processes. A change in the charge distribution should affect the reactions of the (48Al–52Ni)$_{100-x}$(CuO)$_x$ composites. In the (48Al–52Ni)$_{100-x}$(CuO)$_x$ composites, the potential reactions in an argon atmosphere include an Al–Ni intermetallic formation reaction and an Al–CuO thermite reaction. In general, the characteristics of a chemical reaction can be described by the activation energy (E_a) , which can be expressed as [37]:

$$E_a = RT^2 \frac{\mathrm{d}\ln\{k\}}{\mathrm{d}T} \quad (1)$$

where k is the rate constant, T is the temperature, and R is the universal gas constant. An obvious exothermic phenomenon can be detected when k equals a critical value (k_c). Under the same conditions, a smaller E_a indicates that a lower temperature is required if k_c is a constant. It was assumed that the temperature corresponding to k_c is the reaction onset temperature obtained from DSC experiments, i.e., a lower activation energy means a lower reaction onset temperature.

According to previous reports, the activation energy of the intermetallic formation reaction between Al and Ni is 160 kJ/mol [34]. For Al–CuO thermite, the thermite reaction was divided into the Al–CuO (I) and Al–CuO (II) stages, with activation energies of 80 and 260 kJ/mol, respectively [38]. Thus, the Al–CuO (I) reaction, which has the lowest onset temperature among the compounds, should occur first in the (48Al–52Ni)$_{100-x}$(CuO)$_x$ composites, followed by Al–Ni reactions, and then the Al–CuO reaction (II) stage should occur, theoretically. However, the activity of the Al was decreased by the formation of Al_2O_3 on the surfaces, which can be observed in Fig. 3(a). Importantly, due to the electron transfer between CuO and Al and Ni, as discussed above, there were free oxygen atoms with the free state in the CuO lattice that easily vaporized as O_2. Thus, the thermal decomposition expressed in Eq. (2) occurred first in the (48Al–52Ni)$_{100-x}$(CuO)$_x$ composites, resulting in a decrease in the sample mass (Fig. 4(d)) and the generation of Cu_2O (Fig. 3(h) and Fig. 5(d)):

$$\mathrm{CuO} \rightarrow \mathrm{O_2} + \mathrm{Cu_2O} \quad (2)$$

Second, due to its lower binding energy, Al generally has a higher diffusion rate than Ni, which allows the Al atoms to readily gather at the interface between the Al and Ni particles, where the intermetallic formation reaction occurs. Thus, the primary intermetallic formed by the Al–Ni reaction should be Al_3Ni, and the secondary reaction product should be Al_3Ni_2. This should be followed by the thermal decomposition of CuO, and the Al–Ni reactions in the $(48Al–52Ni)_{100-x}(CuO)_x$ composites should take place in the following order, as shown in Fig. 5(c):

$$Al + Ni \rightarrow Al_3Ni \tag{3}$$

$$Al_3Ni + Ni \rightarrow Al_3Ni_2 \tag{4}$$

Finally, when the temperature is high enough to initiate the Al–CuO (II) reaction, the complete aluminothermic reaction as Eq. (5) should occur, as shown in Fig. 5(e).

$$Al + Cu_xO \rightarrow Al_2O_3 + Cu \tag{5}$$

It should be noted that the Cu produced during the reaction can dissolve into the Al_3Ni and Al_3Ni_2 intermetallic lattice and replace Ni due to the same lattice structure (face-centered cubic) and similar atomic radii (Cu, 0.128 nm; Ni, 0.125 nm) [39]. Therefore, the Al_3Ni_2 and Al_3Ni reaction products, along with some Cu, were detected in Fig. 5(e).

Importantly, when CuO was added to the Al–Ni composite, the free electrons in the Al and Ni metals decreased, the reaction activity of the Al–Ni intermetallic formation reaction decreased, and the reaction onset temperature increased. In addition, during the thermal decomposition of the CuO, free oxygen atoms readily diffused through the Al/Ni, Al/CuO and Ni/CuO interfaces because of interface defects and were likely to react with Al and Ni, leading to slight oxidation of the metals. The potentially weak Al–O and Ni–O bonds disturbed the electron distributions in the Al and Ni compared with the composite without the additional free oxygen atoms. Therefore, the free oxygen atoms that originated from the lattice oxygen in the CuO also reduced the number of free electrons in the Al and Ni. As a result, the onset temperature of the intermetallic formation reaction further increased.

The intermetallic formation reaction between the Al and Ni is actually the process of the formation of metal bonds and covalent bonds between Al and Ni. That is, the activity, or the driving force for the intermetallic formation reaction, decreases as the number of free electrons in the metal decreases.

As shown in Fig. 4(a) and Fig. S3, there was a difference in the onset temperatures between the Al–Ni reaction (766 K (Fig. 4(a)) and the Al–CuO reaction (>790 K (Fig. S3)). This difference separated the Al–Ni reaction and the Al–CuO reaction. Their released heat did not impact each other, causing the heat flow (the intensity) of each reaction to only depend on itself. When the onset temperature of the Al–Ni reaction increased as CuO was added, the difference in the onset temperatures between the Al–Ni and Al–CuO reactions decreased, and the heat released by the Al–Ni intermetallic formation reaction induced the Al–CuO thermite reaction effectively. It thus decreased the apparent onset temperature of the Al–CuO reaction. The increased onset temperature of the Al–Ni reaction and the decreased onset temperature in the Al–CuO reaction jointly caused the exothermic temperature zones of the two reactions to overlap, greatly enhancing the instantaneous reaction intensity and reaction rate, which can be represented by the higher heat flow and the shorter reaction temperature region, respectively, as shown in Fig. 4(b–c).

The reaction intensity and reaction rate played a more important role in the energy release behavior of ESMs during high-speed impact than the total amount of released heat. The highly reactive metals Al and Ni can oxidize quickly during high-speed impact in air. Thus, the energy released in the $(48Al–52Ni)_{100-x}(CuO)_x$ composites during high-speed impact in air included contributions from the Al–Ni intermetallic formation reaction and Al–CuO thermite reaction, as well as the oxidation of the Al and Ni, as indicated by the presence of an Al_2O_3 diffraction peak in Fig. 7(a). For the former two reactions, the addition of CuO greatly enhanced the reaction intensity of the Al–Ni system by introducing the thermite reaction and decreasing the difference in the onset temperatures, as discussed above. In fact, the oxidation of the Al and Ni was also affected by the introduction of CuO; more precisely, it was impacted by the increased intensity caused by the introduction of

CuO. According to the Arrhenius equation, the oxidation rate of a metal mainly depends on the environmental temperature. That is, the increased intensity caused by the overlap of the Al–Ni and Al–CuO reactions further accelerated the oxidation of the Al and Ni, resulting in a very elevated energy release and quasi-static peak pressure, which was manifested by an increase in the peak pressure and pressure increase rate with increasing CuO content (Fig. 6(h)). It should be noted that although some gaseous oxygen was released during the annealing process of the $(48Al–52Ni)_{100-x}(CuO)_x$ composites, as discussed above, its contribution to the pressure during high-speed impact was slight and can be neglected. (A detailed discussion can be seen in the supplementary information.)

5. Conclusions

In this work, the effect of CuO on the reaction behaviors of an Al–Ni system was systematically studied through DSC, heat treatment, and ballistic tests. When CuO was added into the Al–Ni system, the microstructure and mechanical properties of the composites exhibited little change due to the clusters of CuO particles. Moreover, the presence of CuO decreased the number of free electrons in the Al and Ni. The decreased number of free electrons, as well as the weak metal-oxygen bonds at the Al/Ni interfaces caused by the thermal decomposition of CuO, postponed the intermetallic formation reaction, and thereby decreased the difference in the onset temperatures between the Al–Ni intermetallic formation and Al–CuO thermite reactions. The heat from the intermetallic formation reaction ignited the thermite reaction and then accelerated the oxidation of Al and Ni, leading to an increased energy release during the heat treatment and ballistic tests. Therefore, the addition of CuO enhanced the reaction intensity of the Al–Ni composite. Importantly, this work demonstrated that the addition of a metal oxide indeed improved the performance of the Al–Ni composite system as an ESM by altering the electron distribution as well as the reaction onset temperatures and reaction intensities.

Acknowledgements

This work has been supported by the National Natural Science Foundation of China (No. 11972372).

Appendix A. Supplementary information

Supplementary materials include the morphologies of the raw powder (Fig. S1), elemental mapping images of the hot-pressed composites (Fig. S2), quasi-static compressive properties (Fig. S3), XRD pattern of the Al–CuO composite annealed at 790 K (Fig. S4), microstructure of the unreacted fragments (Fig. S5) and effects of CuO thermal decomposition on pressure change.

References

[1] E. L. Dreizin, M. Schoenitz, Correlating ignition mechanisms of aluminum-based reactive materials with thermoanalytical measurements, Prog. Energ. Combust., 50 (2015) 81-105.

[2] D. L. Hastings, E. L. Dreizin, Reactive structural materials: Preparation and characterization, Adv. Eng. Mater., 20 (2018) 1700631.

[3] F. Y. Xu, Q. B. Yu, Y. F. Zheng, M. A. Lei, H. F. Wang, Damage effects of double-spaced aluminum plates by reactive material projectile impact, Int. J Impact Eng., 104 (2017) 13-20.

[4] D. L. Hastings, M. Schoenitz, E. L. Dreizin, High density reactive composite powders, J. Alloy. Compd., 735 (2018) 1863-1870.

[5] B. B. Aydelotte, Fragmentation and reaction of structural energetic materials, PhD Thesis, Georgia Institute of Technology, Atlanta, GA, 2013.

[6] M. D. Tucker, Characterization of impact initiation of aluminum-based intermetallic-forming reactive materials, MS Thesis, Georgia Institute of Technology, Atlanta, GA, 2011.

[7] H. Wang, Y. Zheng, Q. Yu, Z. Liu, W. Yu, Impact-induced initiation and energy release behavior of reactive materials, J. Appl. Phys., 110 (2011) 074904.

[8] Y. Wang, W. Jiang, X. Zhang, H. Liu, Y. Liu , F. Li, Energy release characteristics of impact-initiated energetic aluminum–magnesium mechanical alloy particles with nanometer-scale structure, Thermochim. Acta. 512 (2012) 233-239.

[9] W. Xiong, X. F. Zhang, Y. Wu, Y. He, C.T. Wang, L. Guo, Influence of additives on microstructures, mechanical properties and shock-induced reaction characteristics of Al/Ni composites, J. Alloy. Compd., 648 (2015) 540-549.

[10] J. Zhou, Y. He, Y. He, C. T. Wang, Investigation on Impact Initiation Characteristics of Fluoropolymer-matrix Reactive Materials, Propell. Explos. Pyrot., 42 (2017) 603-615.

[11] G. Xanthopoulou, Oxide catalysts for pyrolysis of diesel fuel made by self-propagating high-temperature synthesis (SHS): Part II: Fe–Cr oxide catalysts based on chromite concentrates, Appl. Catal. A: Gen., 187 (1999) 79-88.

[12] A. Maznoy, A. Kirdyashkin, V. Kitler, N. Pichugin, V. Salamatov, K. Tcoi, Self-propagating high-temperature synthesis of macroporous B2+ L12 Ni-Al intermetallics used in cylindrical radiant burners, J. Alloy. Compd., 792 (2019) 561-573.

[13] A. Coverdill, C. Delaney, A. Jennrich, H. Krier, N. G. Glumac, Tungsten Combustion in

Explosively Initiated W/Zr Mechanical Alloys, J. Energ. Mater., 32 (2014) 135-145.

[14] A. L. Kuhl, H. Reichenbac, Combustion effects in confined explosions. Proceedings of the combustion institute, P. Combust. Inst., 32 (2009) 2291-2298.

[15] W. Xiong, X. F. Zhang, M. T. Tan, C. Liu, X. Wu, The Energy Release Characteristics of Shock-Induced Chemical Reaction of Al/Ni Composites, J. Phys. Chem. C, 120 (2016) 24551-24559.

[16] Y. Horie, R. A. Graham, I. K. Simonsen, Synthesis of nickel aluminides under high-pressure shock loading, Mater. Lett., 3 (1985) 354-359.

[17] B. A. Mason, T. R. Sippel, L. J. Groven, I. E. Gunduz, S. F. Son, Combustion of mechanically activated Ni/Al reactive composites with microstructural refinement tailored using two-step milling, Intermetallics, 66 (2015) 88-95.

[18] S. Fischer, M. Grubelich, A survey of combustible metals, thermites, and intermetallics for pyrotechnic applications, in 32nd Joint Propulsion Conference and Exhibit. 1996.

[19] B. E. Homan, K.L. McNesby, J. Ritter, J. Colburn, A. Brant, Characterization of the combustion behavior of aluminum-nickel based reactive materials, Report, U.S. Army Research Laboratory, 2009.

[20] Y. Ohkura, S. Y. Liu, P. M. Rao, X. L. Zheng, Synthesis and ignition of energetic CuO/Al core/shell nanowires, P. Combust. Inst., 33 (2011) 1909-1915.

[21] L. Glavier, G. Taton, J. M. Ducéré, V. Baijot, S. Pinon, T. Calais, A. Estève, M. D. Rouhani, C. Rossi, Nanoenergetics as pressure generator for nontoxic impact primers: comparison of Al/Bi_2O_3, Al/CuO, Al/MoO_3 nanothermites and Al/PTFE, Combust. Flame, 162 (2015) 1813-1820.

[22] S. G. Hashemabad, T. Ando, Ignition characteristics of hybrid Al–Ni–Fe_2O_3 and Al–Ni–CuO reactive composites fabricated by ultrasonic powder consolidation, Combust. Flame, 162 (2015) 1144-1152.

[23] S. W. Dean, J. K. Potter, R. A. Yetter, T. J. Eden, V. Champagne, M. Trexler, Energetic intermetallic materials formed by cold spray, Intermetallics, 43 (2013) 121-130.

[24] R. G. Ames, Energy release characteristics of impact-initiated energetic materials, MRS Online Proceedings Library Archive, 2005, 896.

[25] C. Chen, S.J. Splinter, T. Do, N. S. McIntyre, Measurement of oxide film growth on Mg and Al surfaces over extended periods using XPS, Surf. Sci., 382(1997) L652-L657.

[26] R. Brajpuriya, T. Shripathi, Investigation of Fe/Al interface as a function of annealing temperature using XPS, Appl. Surf. Sci., 2009. 255(12): p. 6149-6154.

[27] J. A. Rotole, P. M. Sherwood, Corrundum (α-Al_2O_3) by XPS, Surf. Sci. Spectra, 5 (1998) 11-17.

[28] M. Chen, X. Wang, Y. H. Yu, Z. L. Pei, X. D. Bai, C. Sun, R. F. Huang, L. S. Wen, X-ray photoelectron spectroscopy and auger electron spectroscopy studies of Al-doped ZnO films, Appl. Surf. Sci., 158 (2000) 134-140.

[29] I. Bertóti, M. Mohai, A. Csanády, P. B. Barna, H. Berek, XPS studies on intermetallic phases formed in Al-Ni and Al-Mn thin films, Surf. Interface Anal., 19 (1992) 457-463.

[30] A. N. Mansour, Characterization of NiO by XPS, Surf. Sci. Spectra, 3 (1994) 231-238.

[31] R. G. Ames, Vented chamber calorimetry for impact-initiated energetic materials, AIAA (American Institute of Aeronautics and Astronautics), 2005.

[32] Y. S. Naiborodenko, V. I. Itin, B. P. Belozerov, V. P.Ushakov, Phases and reactive-diffusion kinetics for mixed Al-Ni powders, Soviet Physics Journal, 16 (1973) 1507-1511.

[33] J. D .E. White, R. V. Reeves, S. F. Son, A. S. Mukasyan, Thermal explosion in Al−Ni system:

Influence of mechanical activation, J. Phys. Chem. A, 113(2009) 13541-13547.

[34] A. G. Gasparyan, A. S. Shteinberg, Macrokinetics of reaction and thermal explosion in Ni and Al powder mixtures, Combust. Explo. Shock +, 24 (1988) 324-330.

[35] Y. Yang, D. G. Xu, K. L. Zhang, Effect of nanostructures on the exothermic reaction and ignition of Al/CuO_x based energetic materials, J. Mater. Sci., 47 (2012) 1296-1305.

[36] M. Mursalat, M. Schoenitz, E. L. Dreizin, Effect of premilling Al and CuO in acetonitrile on properties of Al·CuO thermites prepared by arrested reactive milling, Combust. Flame, 214 (2020) 57-64.

[37] R. L. LeRoy, Relation between Arrhenius activation energies and excitation functions, J. Phys. Chem., 73 (1969) 4338-4344.

[38] S. M. Umbrajkar, M. Schoenitz, E. L. Dreizin, Exothermic reactions in Al–CuO nanocomposites, Thermochim. Acta, 451 (2006) 34-43.

[39] R. W. Cooke, R. L. Hexemer, I. W. Donaldson, D. P. Bishop, Dispersoid strengthening of Al–Cu–Mg P/M alloy utilising transition metal additions, Powder Metall., 55 (2012) 191-199.

Figure captions:

Figure 1. Schematic diagram of ballistic tests (a) projectile; (b) ballistic tests.

Figure 2. (a) XRD patterns and BSE images of the hot-pressed $(48Al–52Ni)_{100-x}(CuO)_x$ composites. ((b) x = 0; (c) x = 4; (d) x = 6; (e) x = 10.

Figure 3. XPS patterns of $Al2p_{3/2}$, $Ni2p_{3/2}$, O1s, and Cu2p spectra of $(48Al–52Ni)_{100-x}(CuO)_x$ composites after annealing at 703 and 803 K, respectively. (a–b) $Al2p_{3/2}$; (c–d) $Ni2p_{3/2}$; (e–f) O1s; (g–h) Cu2p.

Figure 4. DSC curves of $(48Al–52Ni)_{100-x}(CuO)_x$ composites ((a) x=0; (b) x=4; (c) x=6) and (d) TG curves of the composites (x=0, 6).

Figure 5. Microstructural features of $(48Al–52Ni)_{100-x}(CuO)_x$ composites. (a) XRD patterns of the composites (x=0, 6) annealed at 770 K; (b) BSE image of the composite (x=6) annealed at 780 K; (c–d) BSE image of the composite (x=6) annealed at 780 K; (e) BSE image of the composite (x=6) annealed at 790 K.

Figure 6. Energy release behaviors under high-speed impact loading. (a–d) Light emission captured by a high-speed camera for the composite (x=4) at 1400 m/s; (e–g) Quasi-static pressure inside test chamber for the composites with x= 0, 4 and 6, respectively; (h) Relationship between peak pressures and the CuO content at 1400 m/s.

Figure 7. (a) XRD patterns of recovered fragment at 1400 m/s; (b–c) BSE images of reacted recovered fragments for the composites with x=0 and 4, respectively.

Highlights

- The energy release performance of Al–Ni composites can be great enhanced by controlling the electron distribution.
- The influence mechanism of metal oxide on the energy release behaviors of Al–Ni composites is firstly investigated from the electron distribution.
- The reaction onset temperature of Al–Ni composites is affected by CuO, which facilitates to lose electrons of Al and Ni.
- The reaction intensity of Al–Ni–CuO composite is effectively tailored by simulating intermetallic-forming and thermite reactions simultaneously.

Declaration of interests

☑The authors declare that they have no known competing financial interests or personal relationships that could have appeared to influence the work reported in this paper.

☐The authors declare the following financial interests/personal relationships which may be considered as potential competing interests: